Author/s:
Saxena, S;Marlow, P;Subbiah, J;Colsmann, A;Wong, WWH;Jones, DJ

Title:
Pyridine End-Capped Polymer to Stabilize Organic Nanoparticle Dispersions for Solar Cell Fabrication through Reversible Pyridinium Salt Formation

Date:
2021-08-04

Citation:
Saxena, S., Marlow, P., Subbiah, J., Colsmann, A., Wong, W. W. H. & Jones, D. J. (2021). Pyridine End-Capped Polymer to Stabilize Organic Nanoparticle Dispersions for Solar Cell Fabrication through Reversible Pyridinium Salt Formation. ACS Applied Materials and Interfaces, 13 (30), pp.36044-36052. https://doi.org/10.1021/acsami.1c07219.

Persistent Link:
https://hdl.handle.net/11343/285511

A Pyridine End-capped Polymer to Stabilize Organic Nanoparticle Dispersions for Solar Cell Fabrication through Reversible Pyridinium Salt Formation

Sonam Saxena,[1] Philipp Marlow,[2,3] Jegadesan Subbiah,[1] Alexander Colsmann,[2,3] Wallace W. H. Wong,*[1,] David J. Jones*[1]

[1]School of Chemistry, Bio21 Institute, University of Melbourne, VIC, 3010 Australia.

E-mail: djjones@unimelb.edu.au

E-mail: wwhwong@unimelb.edu.au

[2]Material Research Center for Energy Systems, Karlsruhe Institute of Technology (KIT), Strasse am Forum 7, 76131, Karlsruhe, Germany

[3]Light Technology Institute, Karlsruhe Institute of Technology (KIT), Engesserstrasse 13, 76131, Karlsruhe, Germany

Keywords: poly(3-hexylthiophene), end-capped polymer, nanoparticle dispersion, bulk heterojunction, organic solar cells

Abstract: Bulk-heterojunction nanoparticle dispersions in water or alcohol can be employed as eco-friendly inks for the fabrication of organic solar cells by printing or coating. However, one major drawback is the need for stabilizing surfactants, which facilitate the nanoparticle formation but later hamper the device performance. When surfactant-free dispersions are formulated, a strong limitation is imposed by the dispersion concentration due to the tendency of nanoparticles to aggregate. In this work, pyridine end-capped poly(3-hexylthiophene) (P3HT-Py) is synthesized and included as an additive for the stabilization of P3HT:indene-C_{60} bis-adduct (ICBA) nanoparticle dispersions. In presence of acetic acid (AcOH), a surface active pyridinium acetate end-capped P3HT ion pair, P3HT-PyH^+AcO^-, is formed which effectively stabilizes the dispersion and hence allows the formation of dispersions with smaller nanoparticle sizes and higher concentrations of up to 30 mg/mL in methanol. The dispersions exhibit an enhanced shelf-lifetime of at least 60 days at room temperature. After the deposition of light-harvesting layers from the nanoparticle dispersions, the ion-pair formation is reversed at elevated temperatures leading to re-generation of P3HT-Py and AcOH. The AcOH evaporates from the active layer, while the performance of the corresponding solar cells is not affected by the residual P3HT-Py in the devices. Enhanced nanoparticle stability is achieved with only 0.017 wt.% pyridine in the P3HT:ICBA formulation.

1. Introduction

Solution-processable organic semiconductors facilitate the roll-to-roll production of light-weight and flexible organic solar cells (OSCs). OSCs commonly comprise blends of donors and acceptors (bulk-heterojunctions) for best light-harvesting and charge carrier transport. Their power conversion efficiency (PCE) has continued to improve in recent years approaching ~18%[1] and ~16%[2] for small-scale and large-scale applications, respectively. Besides designing new light-harvesting compounds, this story of success is underpinned by advancements in the understanding of charge carrier transport and enhancement of the micro-morphology of the bulk-heterojunction which forms upon deposition from solution.[3] To date, in research laboratories, OSCs are mostly fabricated using toxic halogenated solvents, which can be challenging to use at industrial scale due to their health and environmental risks. Thus, in addition to achieving high device performance, eco-friendly processing is a prerequisite for the large-scale production of OSCs.[4] Opting for eco-friendly solvents, however, often brings along the challenge of crafting optimal bulk-heterojunctions.

Depositing layers from nanoparticle (NP) dispersions of organic semiconductors such as conjugated polymers, molecular materials and fullerenes in water or alcohol may pave a promising route to achieve "greener" processing.[5, 6] This technique can become part of an eco-friendly OSC fabrication, and also enables deposition of advanced multi-layer device architectures since the need of solubility is decoupled from solution processing.[7] NP dispersions can be prepared through miniemulsions where the semiconductors are dissolved in organic solvents and then dispersed in water containing surfactants.[8, 9] The surfactants stabilize the surface of the NPs. OSCs fabricated from NPs comprising poly-3-hexylthiophene (P3HT):phenyl-C_{61}-butyric acid methyl ester (PCBM) or P3HT:indene-C_{60} bisadduct (ICBA), stabilized by the surfactant sodium dodecyl sulfate (SDS), achieved PCEs between 1.2% and 2.5%.[10, 11] Similarly, devices from P3HT:*o*-IDTBR blends stabilized with SDS and Pluronic F127 yielded PCEs of 2.73% and

5.23%, respectively.[12] These PCEs are considerably lower than the reported PCEs of devices fabricated using chlorinated solvents. For instance, the PCE of *o*-dichlorobenzene (DCB)-processed devices of P3HT:PCBM and P3HT:ICBA were reported as 5%[13] and 6.5%[14] respectively. The low device performances have been attributed to the persistence of surfactant in the light-harvesting layer, where it can hinder charge carrier transport and extraction.[15] Charge carrier transport is further hampered by the core-shell morphology of NPs prepared through the miniemulsion route, and the subsequent formation of an inefficient polymer-fullerene network.[9] To overcome these limitations, an alternative surfactant-free approach of forming P3HT:ICBA NP dispersions was introduced and a PCE of 4% was achieved.[5] However, in the absence of surfactants, this approach is limited to the formation of NP despersions with low concentrations, which then require multiple coating steps to attain light-harvesting layer thicknesses of about 250 nm.[5] Therefore, NP dispersion with higher concentrations would ease the deposition of sufficiently thick light-harvesting layers with fewer coating steps. Although roll-to-roll-compatible processes such as inkjet printing, spray coating or doctor blading[16] can partly compensate for low concentrations of dispersions, a wider process window opens up if the dispersion concentrations can be increased.

In this work, we investigate a new concept for NP stabilization which allows the elimination of commonly employed surfactants, such as SDS, yielding higher dispersion concentrations, while maintaining device PCE. The fundamental premise of our approach is the reversible reaction of pyridine with weak acids to form pyridinium salts which can act as surface active agents. In this work, small amounts of pyridine end-capped P3HT (P3HT-Py) are added to the semiconductor P3HT:ICBA solution, see Figure 1A. The P3HT-Py converts to pyridinium acetate (P3HT-PyH$^+$AcO$^-$) in presence of acetic acid (AcOH), see Figure 1B. We then expect the resultant surface active ion pair, P3HT-PyH$^+$AcO$^-$, to modify the surface charge of P3HT:ICBA NPs. This would assist the stability against aggregation, and enable the formation of concentrated NP dispersions exhibiting longer shelf-lifetime. An important feature of P3HT-Py is the reversibility of the P3HT-PyH$^+$AcO$^-$ ion pair formation, see Figure 1B. After deposition of the light-harvesting layer from the stabilized NP dispersion, thermal annealing at 120 °C or above decomposes the P3HT-PyH$^+$AcO$^-$ leading to regeneration of P3HT-Py and AcOH, followed by the evaporation of the latter.[17] The use of NP dispersions to form the light-harvesting layers and the performance of the corresponding OSCs are investigated.

2. Results and discussions

2.1 Synthesis of P3HT-Py

The required mono-brominated P3HT, P3HT (Br/H), was synthesized using standard Grignard metathesis (GRIM) polymerization.[18] The P3HT-Py was then obtained via a Suzuki-Miyaura coupling of synthesized P3HT-(Br/H) and pyridine boronic acid.[19] P3HT-Py with a small number average molecular weight, M_n = 5,000 g/mol, was targeted to, i) ensure a sufficent length of the P3HT-Py to mix with the P3HT in the light-harvesting layer, ii) be short enough to promote mobility/diffusion in the annealed layer, and iii) facilitate characterization, especially end-group verification, see Scheme 1.

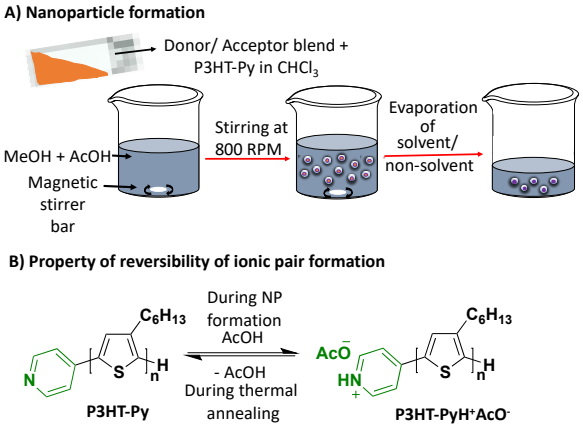

Figure 1: A) Schematic of the P3HT:ICBA NP preparation in MeOH (non-solvent), B) conversion of P3HT-Py into the ionic pair P3HT-PyH$^+$AcO$^-$ in presence of AcOH, assisting the stabilization of P3HT:ICBA NPs. During thermal treatment of the NP layers, P3HT-PyH$^+$AcO$^-$ can be decomposed to regenerate P3HT-Py with the complete removal of AcOH.

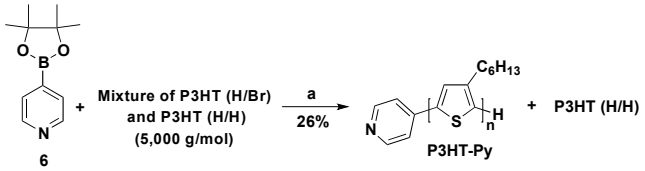

Scheme 1: Synthesis of P3HT-Py, (a) 10 mol% $Pd(PPh_3)_4$, 2M K_2CO_3 (aq.) (5 mL), THF (10 mL), 90 °C, overnight.

Notably, acid quenched P3HT synthesized via GRIM polymerization usually results in the desired P3HT (Br/H) as well as a hydrogen terminus at both ends of the polymer chain, P3HT (H/H). To achieve a sample with high end group fidelity, the P3HT (H/H) fraction must be removed. P3HT (H/H) removal involved the treatment of the crude P3HT-Py mixture with *p*-toluene sulfonic acid (tosylic acid, TsOH) to generate the pyridinium salt. The P3HT-PyH$^+$ tosylate (P3HT-PyH$^+$*p*-TsO$^-$) was then dry-loaded onto silica and eluted with chloroform ($CHCl_3$). It was anticipated that pyridinium salt of P3HT-Py would associate strongly with silica compared to P3HT (H/H), enabling chromatographic separation. However, this idea of removing P3HT (H/H) did not work as expected and most of the fractions were the combination of P3HT-PyH$^+$*p*-TsO$^-$ and P3HT (H/H). This may be attributed to the pyridine being a small functional group at the end of a long P3HT chain creating only slight difference in P3HT-PyH$^+$ and P3HT (H/H) polarities. Therefore,

multiple cycles of purification were required, purifying 50 mg of polymer mixture at a time. Consequently, even after achieving complete conversion of P3HT-Br to P3HT-Py, only 25% to 30% of the P3HT-PyH$^+$*p*-TsO$^-$ was recovered in each cycle of purification. The P3HT-Py was obtained by treating the isolated P3HT-PyH$^+$*p*-TsO$^-$ with aqueous sodium hydroxide (NaOH) and the resultant polymer was washed thoroughly with water using liquid-liquid extraction technique.

2.2 Structural characterization of P3HT-Py

^{1}H NMR spectroscopy was used to assess the purity and to determine M_n of the synthesised P3HT-Py. The ^{1}H NMR spectrum of P3HT-Py sample is presented in Figure 2A between 2.4 and 9.5 ppm, while the ^{1}H NMR spectrum of the P3HT (Br/H) precursor is presented in Figure S1 (Supporting Information). The relative ratio of protons resonating at 2.6 ppm (methylene protons a and b') and 2.8 ppm (methylene protons d) for P3HT (Br/H) was determined, giving the degree of polymerization DP_n = 28. Multiplying DP_n with the mass of the repeating unit (166.3 g/mol) resulted in M_n= 4,656 g/mol of P3HT.

In Figure 2A, the presence of two broad peaks at 7.4 and 8.7 ppm (aromatic region) in the ^{1}H NMR spectrum (see Figure S2 for full spectrum, Supporting Information) corresponds to the pyridine group in P3HT-Py. The integral of these peaks (e" and f") in Figure 2A was set to 2 and the relative integral for aromatic thiophene protons (c) was calculated to be 28.5. This is consistent with the estimated DP_n = 28 above, confirming the separation of P3HT-Py (99% pure) from P3HT (H/H). Note that, we expected the observation of two doublets for pyridine end-group in the aromatic region of the ^{1}H NMR spectrum of P3HT-Py. Instead, two broad peaks with poor splitting were observed due to smaller wt.% (1.7 wt.%) of pyridine in P3HT-Py. The total wt.% of Py in P3HT-Py was calculated as ((Molecular wt. of Py)/(M_n of P3HT-Py) × 100). The M_n estimated from ^{1}H NMR of P3HT and P3HT-Py was of the same order of the molecular weights obtained from gel permeation chromatography (GPC), M_n= 5,600 g/mol (see Figure S3, Supporting Information).

Matrix Assisted Laser Desorption Ionization- Time of Flight Mass Spectrometer (MALDI-TOF MS) analysis was performed on P3HT and P3HT-Py. The ratio of Br/H and H/H ends of P3HT was estimated to be ~ 85:15 (see Figure S4, Supporting Information). In Figure 2B, the MALDI-TOF spectrum of P3HT-Py showed only one series of mass peaks assigned to P3HT-Py, confirming the presence of the pyridine end group. The peaks in the spectrum correspond to the sum of the molar masses (g/mol) of the monomer repeat unit (166.3 × n, n=13-22) + pyridine end-group + 1 hydrogen atom. For example, the m/z of purified P3HT-Py equals 166.3×17 + 78.09 + 1.08 = 2906.3 for one of the peaks. The M_n calculated for P3HT-Py from MALDI-TOF spectrum was 3,070 g/mol (see Supporting Information).

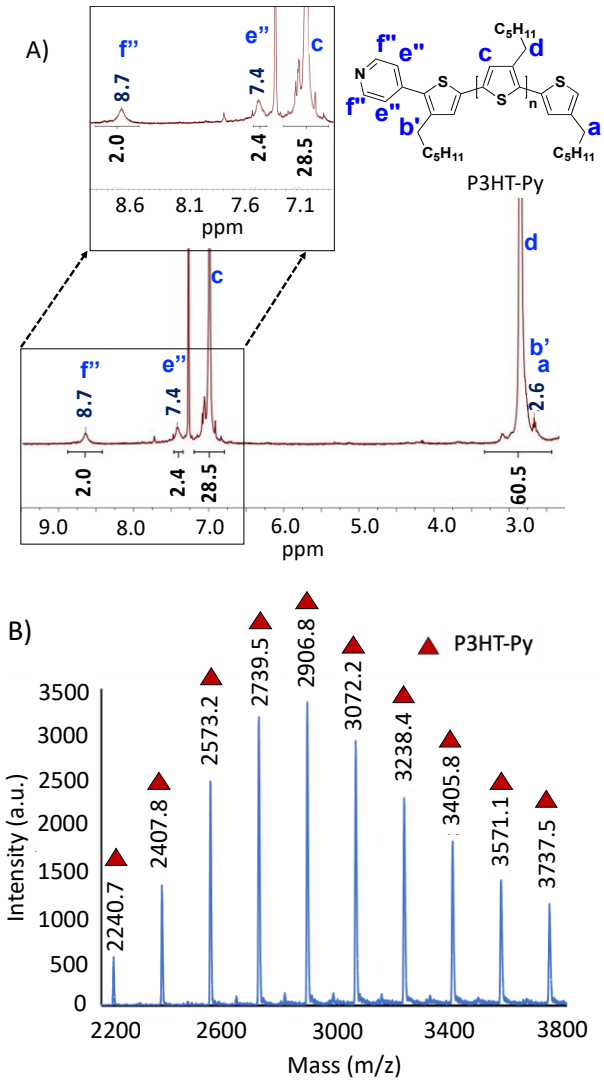

Figure 2: A) ^{1}H NMR spectrum of P3HT-Py in $CHCl_3$ and B) MALDI-TOF spectrum of P3HT-Py (p-(3HT)n-Py, n=13-22).

2.3 Nanoparticle formation and stability

To investigate the nanoparticle formation, a mixture of commercially available P3HT and ICBA (1:1 wt:wt) was dissolved in chloroform (solvent) with a concentration of 1 mg/mL. To this chloroform solution, a measured amount of P3HT-Py was added. NPs were prepared by the rapid addition of the chloroform solution into MeOH (non-solvent) containing AcOH (final $CHCl_3$:MeOH, 1:4 v:v). Since chloroform and MeOH are miscible, but P3HT, ICBA and P3HT-Py are insoluble in MeOH, the solubility of the semiconductors is reduced immediately upon mixing, triggering the formation of NPs. Finally, the solution volume was reduced by removing chloroform and some of the MeOH to yield the desired NP concentration in MeOH. Dynamic light scattering (DLS) was then used to determine the size distribution of the NPs in the MeOH dispersion.

Initial experiments studied the concentration of P3HT-Py and AcOH for best stabilization of the P3HT:ICBA NP dispersions. A series of NP dispersions were formed by

adding varying amounts of P3HT-Py (2 to 7 wt.% with respect to the total mass of P3HT) to the chloroform solution of P3HT:ICBA. For instance, to prepare NP dispersions with a concentration of 1 mg/mL using 2 wt.% of P3HT-Py and AcOH, 0.01 mg of P3HT-Py was added to the 1 mg/mL chloroform solution of P3HT:ICBA and 0.01 mg of AcOH was added to MeOH. The wt.% of Py in 2 wt.% of P3HT-Py is 0.017, achieved by multiplying the total wt.% of Py in P3HT-Py (1.7 wt.%) and the mass of P3HT-Py added for NP formation (in this case 0.01 mg). To achieve such small additive quantities, diluted stock solutions were used (see experimental details Section 4 for the exact amounts added). The P3HT-Py:AcOH ratio for all these experiments was kept at 1:1. It was anticipated that the P3HT-PyH$^+$ and AcO$^-$ ion pairs will accumulate on the surface of NPs preventing their agglomeration, thus resulting in stable dispersions.

In aqueous dispersions, stabilization is commonly quantified by measuring the zeta-potential. However, these measurements yield ambiguous data in alcoholic dispersions, therefore, NP stabilization has to be assessed differently. We assessed the stability of dispersions by using the size and temporal stability of the NPs, with smaller NP sizes indicating more stable dispersions. In addition, small NP sizes suggest that the Ostwald ripening does not occur in dispersions, which is also indicative of NP stability.

In Table 1, the properties of these NP dispersions are presented, with average sizes of the NPs reducing from 112 nm to 77 nm as the wt.% of P3HT-Py and AcOH increases from 2 to 7 wt.%. See Figure S5 (Supporting Information) for the related DLS plots. As the wt.% of P3HT-Py increases, the maximum potential number of P3HT-PyH$^+$ and AcO$^-$ ion pairs at the surface of NPs also increases, leading to either more stable NPs, or the ability to stabilise a greater surface area, *i.e.* a reduction of the NP size. Control experiments with the addition of either only P3HT-Py or only AcOH confirmed that both additives were needed for NP stabilization, see Table S1 (Supporting Information). We chose to perform further experiments using 3 wt.% loading of P3HT-Py and AcOH. Although larger P3HT-Py/AcOH loadings yielded slightly smaller NPs, the larger amounts of P3HT-Py may affect the molecular packing of P3HT which would in turn negatively affect the performance of solar cells.

In a second series of experiments, with the aim to eventually reducing the number of process steps during light-harvesting layer deposition, we targeted higher NP concentrations by increasing the semiconductor concentration of P3HT:ICBA in the initial chloroform solutions. While maintaining a 3 wt.% of P3HT-Py and AcOH, final P3HT:ICBA NP dispersions of concentrations 10, 20 and 30 mg/mL were achieved exhibiting NP sizes of 101 ± 1 nm, 106 ± 3 nm and 112 ± 2 nm with $Đ_{np}$ = 0.07, 0.05 and 0.03, respectively, see Table S2 (Supporting Information).

Table 1: NP size in MeOH *versus* P3HT-Py concentration. The size and its standard deviation were calculated from 3 DLS measurements (10 runs each). $Đ_{np}$ represents the dispersity of NPs.

Wt.% of P3HT-Py and AcOH	$Đ_{np}$	**Size (nm)**
0%	0.06	112 ± 3.2
2%	0.04	84 ± 1.5
3%	0.04	82 ± 0.4
4%	0.05	81 ± 0.7
5%	0.07	78 ± 1.3
6%	0.07	77 ± 0.3
7%	0.05	77 ± 0.5

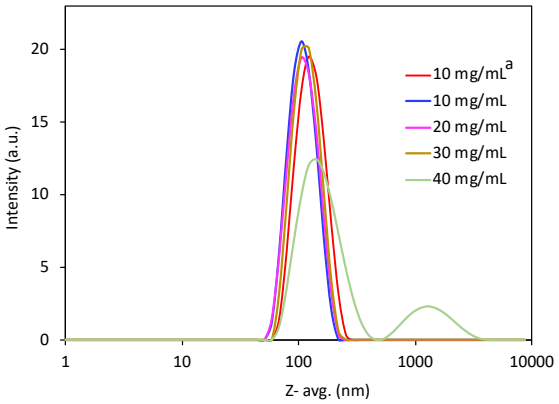

Figure 3: Particle size distributions of P3HT:ICBA NP dispersions in MeOH at concentrations 10, 20, 30 and 40 mg/mL prepared without (legend entry includes superscript 'a') and with addition of 3 wt.% P3HT-Py and AcOH.

We also attempted to prepare dispersions of concentration 40 mg/mL using 3 wt.% of P3HT-Py and AcOH, see Figure 3. However, DLS measurements on this dispersion returned a substantially larger average NP size of 163 ± 2.0 nm indicating partial agglomeration of the NPs, and hence marking the limit of the stabilization support provided by the P3HT-PyH$^+$AcO$^-$ ion pair in this set of experiments. For reference, we also formed NP dispersions without P3HT-Py and AcOH. Dispersions prepared with a concentration of 10 mg/mL without the support of ion pair exhibited a NP diameter of 120 ± 2 nm and $Đ_{np}$ = 0.06. In attempts to prepare non-stabilized NP dispersions with concentrations 20 and 30 mg/mL, the semiconductors precipitated immediately after addition of their chloroform solution into methanol.

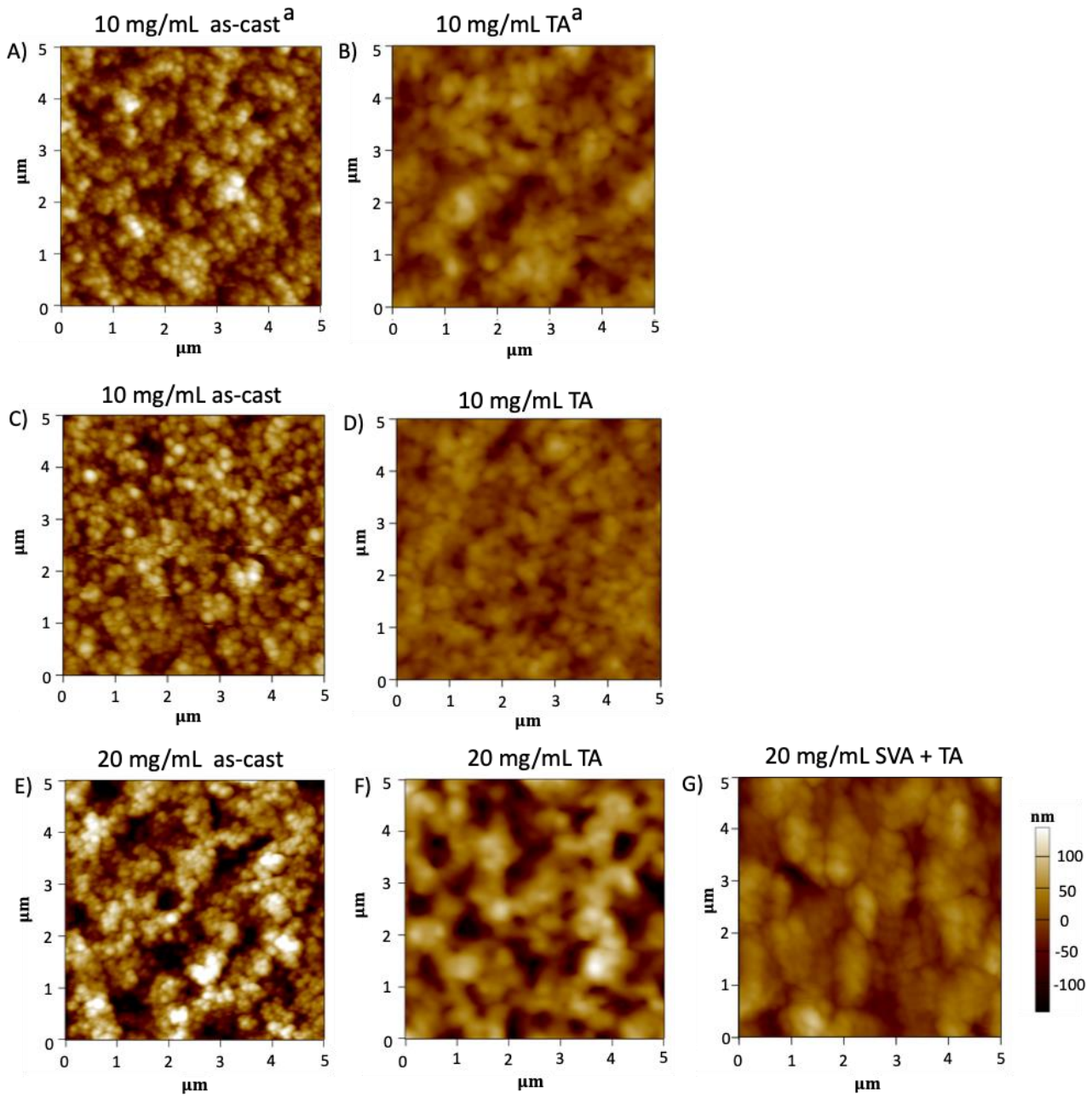

Figure 4: AFM topography images (5µm × 5µm) of as-cast and thermally annealed (TA, 150 °C for 10 min) nanoparticulate layers spin cast from P3HT:ICBA (1:1) dispersions of different concentrations in MeOH (A-G). Dispersions prepared without addition of 3 wt.% P3HT-Py and AcOH (denoted with superscript 'a' at the top of the images) - A) 10 mg/mL, as-cast and B) 10 mg/mL, TA. Dispersions prepared by adding 3 wt.% P3HT-Py and AcOH - C) 10 mg/mL, as-cast, D) 10 mg/mL, TA, E) 20 mg/mL, as-cast, F) 20 mg/mL, TA, and G) 20 mg/mL, solvent vapor annealed (SVA) with dry THF (20 s) followed by TA.

This demonstrates that addition of P3HT-Py and AcOH and the subsequent formation of P3HT-PyH^+AcO^- ion pair can provide enhanced NP stability. The enhanced stability of the NP dispersions was not only observed in smaller NP sizes but also in a good shelf-lifetime. NP dispersion stability can be monitored by comparing the absolute UV-Vis absorption of the samples over time. Any precipitated NPs can be filtered out of a diluted stock solution (50 µl stock dispersion into 1 mL of MeOH) using a 0.22 µm syringe filter, resulting in a lower absolute UV-Vis absorption if NPs are removed. We examined the stability of 20 mg/mL NP dispersions, stabilized with the assistance of P3HT-PyH^+AcO^- at day 1, day 15, and day 60, see Figure S6 (Supporting Information). The effectiveness of P3HT-PyH^+AcO^- ion pair in NP stabilization was demonstrated as the dispersions of 20 mg/mL stabilized by this ion pair showed only 26% absorbance reduction on day 60, see Figure S6 (Supporting Information).

2.4 Thin-film properties

To prepare for the later fabrication of solar cells from P3HT-PyH^+AcO^- stabilized P3HT:ICBA NP dispersions, the conditions required to spin cast 250 nm thick (target thickness) nanoparticulate layers on glass substrates were

examined. This thickness was chosen as it provided best efficiencies for the devices fabricated using surfactant-free 10 mg/mL NP dispersions in the previous work.[5] The thin-film thicknesses were measured using a tactile stylus profiler, and the results are listed in Table 2. Using the 10 and 20 mg/mL NP dispersions, eight and three coating steps were needed, respectively, to achieve the target thickness. Using the 30 mg/mL dispersion, 220 nm thick nanoparticulate layers were achieved with 2 coating steps. However, preliminary testing of solar cells prepared from 30 mg/mL showed inconsistent results. Further optimization is required to work with 30 mg/mL dispersions, and this is part of our ongoing work. In the current work, the thin-film properties and the subsequent device fabrication process will be presented for NP dispersions of concentration up to 20 mg/mL.

Atomic force microscopy (AFM) was used to investigate the surface roughness of the thin films. The NPs become clearly visible in the AFM images of all as-cast layers prepared from 10 and 20 mg/mL P3HT-PyH$^+$AcO$^-$ stabilized NP dispersions, see Figure 4. The root-mean-square roughness R_q of the as-cast layers was 40 nm (10 mg/mL) and 64 nm (20 mg/mL), see Figure 4C and 4E, respectively. The higher roughness of the latter films may be attributed to an enhanced tendency for aggregation in more concentrated dispersions. The layers were thermally annealed (150 °C, 10 min) to join the NPs for more efficient charge carrier extraction into the electrodes and less bimolecular charge carrier recombination on electrically isolated individual nanoparticles.[5] After thermal annealing, the homogeneity of the layers improved and R_q dropped to 20 nm (10 mg/mL) and 44 nm (20 mg/mL), see Figure 4D and 4F, respectively. To further improve the homogeneity of the layers prepared from 20 mg/mL dispersions, an additional step of solvent vapor annealing (SVA) in THF atmosphere (20 s) was introduced before thermal annealing, yielding R_q = 32 nm, see Figure 4G.

For reference, we also investigated layers cast from 10 mg/mL dispersions without the use of P3HT-PyH$^+$AcO$^-$ which have been reported previously.[5] The R_q before annealing was 41 nm which was reduced to 28 nm after annealing, see Figure 4A and 4B, respectively. Comparing this result with the roughness of layers deposited from P3HT-PyH$^+$AcO$^-$ stablized NP dispersions suggests that the P3HT-Py is not detrimental to the final thin-film formation. As P3HT:ICBA NP dispersion concentrations above 10 mg/mL could not be achieved omitting stabilizing agents in this work or previously, no comparative AFM data is available.

In the final step, we demonstrate that upon thermal annealing the pyridinium acetate is decomposed followed by a complete removal of AcOH from the thin film leaving behind P3HT-Py in its original form. This was demonstrated by performing infrared (IR) spectro-

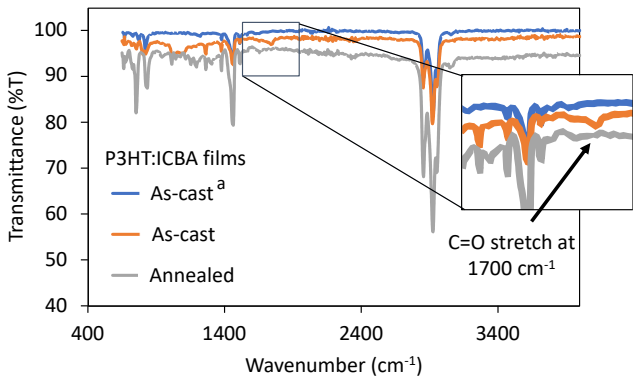

Figure 5: IR spectrum of as-cast and thermally annealed (150 °C, 10 min) P3HT:ICBA (1:1) NP layers deposited from NP dispersions prepared without (legend entry includes superscript 'a') and with addition of 3 wt.% P3HT-Py and AcOH.

scopy measurements on two samples with layers spin coated (1000 rpm, 3 coatings) from P3HT-PyH$^+$AcO$^-$ stabilized P3HT:ICBA NP dispersions (20 mg/mL). One sample was annealed at 150 °C for 10 min, while the other sample was investigated as-cast. The IR spectrum of the as-cast layer showed the presence of acetate, represented by the C=O stretch at 1780 cm^{-1}, see Figure 5. In the annealed layer, the C=O absorption band was missing, indicating thermal decomposition of the pyridinium acetate and removal of AcOH.[17] Direct detection of the pyridine end-cap is not possible as there is no strong absorption wavelength for detection at its final concentration of 0.5 wt.% in the thin film.

The performance of OSCs strongly depends on the development of the bulk-heterojunction morphology, that is a well-crafted, bi-continous inter-penetrating network of polymers and fullerenes. For P3HT-based devices, semi-crystalline domains appear to correlate with high performance. This would contribute to better charge carrier transport through the polymer and at the same time reduction in bandgap for better light-harvesting.

The absorption spectra of P3HT:ICBA reference layers as cast from DCB exhibit distinct vibronic peaks at 510 nm, 560 nm and 610 nm corresponding to 0-2, 0-1 and 0-0 transitions to the vibronic modes of the excited electronic state of P3HT, see Figure 6A. The appearance of these vibronic features in thin films indicates the formation of semi-crystalline P3HT domains through π–π stacking, which is essential for the transport of photogenerated holes to the electrodes. Consistent with the literature,[20-22] these vibronic features are more pronounced in the as-cast nanoparticulate layers than in the reference layers cast from DCB solution, indicating the formation of ordered P3HT domains already during nanoparticle synthesis[23], which then also translates to the NP layers. Often, the performance of bulk-heterojunctions comprising P3HT can be improved by thermal annealing or SVA. Upon thermal annealing, we found enhanced vibronic features of P3HT in the reference layers deposited from DCB, and the absorption spectra showed significant red-shift of the

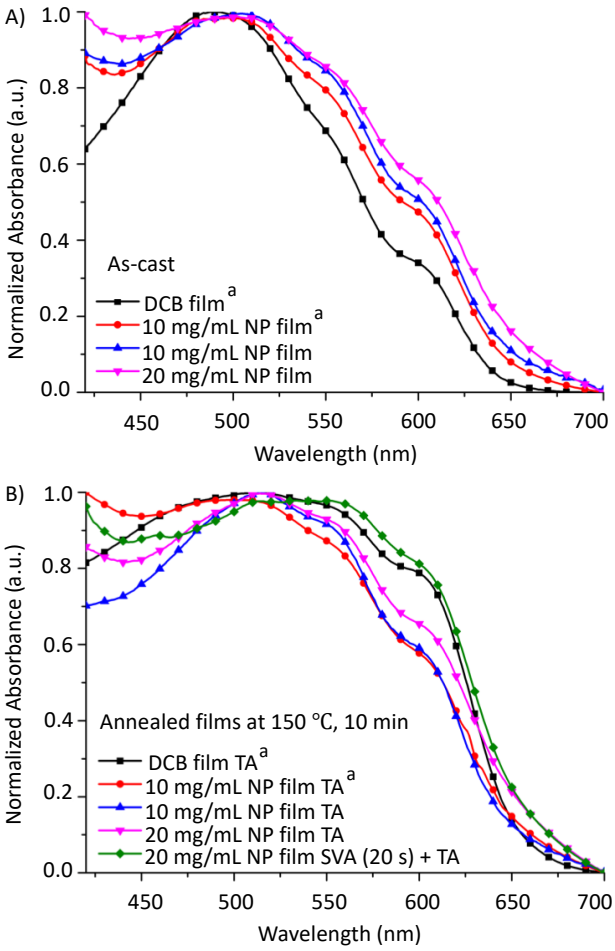

Figure 6: Normalized UV-Vis absorption spectra of P3HT:ICBA (1:1 w/w) layers spin cast from NP dispersions and, for reference, DCB solution. A) As-cast layers and B) thermally annealed (TA) layers (150 °C for 10 min); solvent vapor annealing (SVA, dry THF, 20 s) was used to further improve the results. The superscript 'a' in the legend entries indicates that the layers were formed from NP dispersions prepared without addition of 3 wt.% P3HT-Py and AcOH.

absorption, indicating a reorganization of P3HT for a higher degree of π–π stacking, see Figure 6B. This effect is less pronounced in the nanoparticulate thin-films which already exhibited a high degree of π–π stacking before the annealing step. Best results were achieved with the combination of thermal annealing and SVA in THF atmosphere (20 s). Notably, the very similar film forming properties of P3HT-PyH$^+$AcO$^-$ stabilized and non-stabilized dispersions indicate that the employment of P3HT-Py and AcOH does not affect the known film forming mechanisms in P3HT:ICBA nanoparticulate thin films, which is an important prerequisite to proceed with the fabrication of solar cells.

2.5 Photovoltaic performance

The P3HT-Py additive will remain in the light-harvesting layer at the end of device assembly and, therefore, it is essential to investigate if the presence of the P3HT-Py has any detrimental influence on the device performance.

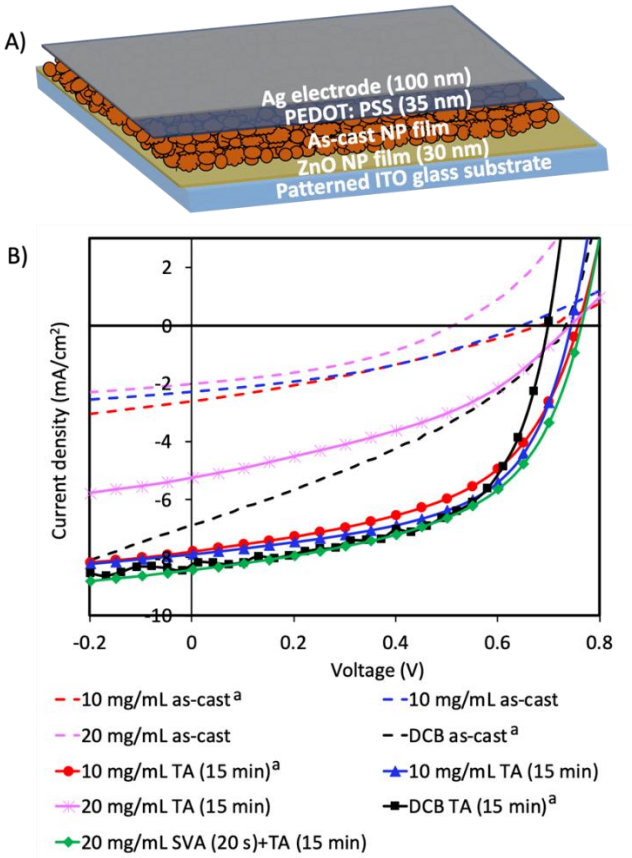

Figure 7: A) OSC architecture used in this work, B) J-V curves of P3HT:ICBA NP solar cells. Dashed lines and solid lines represent as-cast and annealed light-harvesting layers, respectively. TA for 15 min included thermal annealing of the light-harvesting layer for 10 min followed by PEDOT:PSS deposition which was further annealed for 5 min. The SVA (20 s) + TA (15 min) included solvent vapor annealing of the light-harvesting layer with dry THF for 20 s, TA for 10 min, and another TA for 5 min after PEDOT:PSS layer deposition. The superscript 'a' in the legend entries indicates that the light-harvesting layers were deposited from dispersions which were prepared without the assistance of 3 wt.% of P3HT-Py and AcOH.

OSCs with inverted device architecture comprising zinc oxide (ZnO, 30 nm), P3HT:ICBA (250 nm), PEDOT:PSS (35 nm) and a silver electrode (Ag, 100 nm) were fabricated on patterned indium tin oxide (ITO) glass substrates, see Figure 7A. The current density-voltage (*J-V*) curves of the OSCs were recorded under AM 1.5 illumination, see Figure 7B. Their performance data are summarised in Table 2.

All as-cast nanoparticulate devices (dashed lines) produced low short-circuit current densities (J_{sc}) which were improved upon thermal annealing of the light-harvesting layer (150 °C, 10 min, before cathode deposition). Thermal annealing also improved the open-circuit voltage (V_{oc}) and the fill factor (FF) resulting in a significant overall enhancement of the PCE. Notably, upon annealing, the devices assembled from 10 mg/mL

Table 2: Solar cell fabrication parameters and corresponding device performance (at least 8 devices were measured per entry). "C.S" represents the number of coating steps required for light-harvesting layer deposition. TA for 15 min includes thermal annealing of the light-harvesting layer at 150 °C for 10 min followed by PEDOT:PSS deposition which was further annealed at 150 °C for 5 min. The SVA (20 s) + TA (15 min) includes solvent vapor annealing of the light-harvesting layer with dry THF for 20 s, TA at 150 °C for 10 min, and finally, TA at same temperature for 5 min after depositing the PEDOT:PSS layer.

	Conc. (mg/mL)	Wt.% of P3HT-Py and AcOH	C.S	Film treatment	Film thickness (nm)	V_{oc} (V)	J_{sc} (mA/cm^2)	FF	% PCE
DCB solution	30	0	1	As cast	201 ± 10	0.7 ± 0.1	6.9 ± 0.2	34 ± 3	1.7 ± 0.1
	30	0	1	TA (15 min)	168 ± 16	0.7 ± 0.2	8.2 ± 0.1	64 ± 2	3.6 ± 0.1
NP dispersion	10	0	8	As cast	350 ± 13	0.7 ± 0.1	2.5 ± 0.3	30 ± 2	0.5 ± 0.1
	10	0	8	TA (15 min)	250 ± 5	0.8 ± 0.1	7.7 ± 0.2	47 ± 1	3.0 ± 0.1
	10	3	8	As cast	380 ± 9	0.6 ± 0.3	2.2 ± 0.2	36 ± 3	0.5 ± 0.1
	10	3	8	TA (15 min)	271 ± 5	0.8 ± 0.1	8.0 ± 0.1	49 ± 2	3.1 ± 0.2
	20	3	3	As cast	371 ± 14	0.5 ± 0.1	2.0 ± 0.1	35 ± 2	0.3 ± 0.1
	20	3	3	TA (15 min)	260 ± 3	0.7 ± 0.1	5.2 ± 0.1	40 ± 1	1.5 ± 0.1
	20	3	3	SVA (20 s) + TA (15 min)	247 ± 11	0.8 ± 0.1	8.4 ± 0.2	54 ± 1	3.5 ± 0.2

dispersions prepared with and without addition of 3 wt.% P3HT-Py and AcOH exhibited similar J_{sc}. This observation suggested that the P3HT-Py had little-to-no impact on the electronic properties of the bulk-heterojunction.

The devices made from 20 mg/mL dispersions exhibited reduced J_{sc} and V_{oc} in comparison to the OSCs made from 10 mg/mL dispersions (with and without 3 wt.% P3HT and AcOH). The combination of SVA and thermal treatment resulted in smoother and more compact layers which resulted in enhanced device performance. Table 2 illustrates that the J_{sc} of devices fabricated using 20 mg/mL dispersions increased to 8.4 mA/cm^2 and the PCE reached 3.5% which was similar to the performance of devices deposited from DCB solution in this work.

3. Conclusion

We reported on a novel stabilization mechanism for P3HT:ICBA NPs which involved adding small amounts of pyridine end-capped P3HT (P3HT-Py) to the bulk-heterojunction. In presence of AcOH, the P3HT-Py converts to P3HT-PyH$^+$AcO$^-$ ion pair, enabling formation of NPs with higher stability and smaller diameter. Adding only 3 wt.% of a P3HT carrier polymer with pyridine attached we could effectively stablize NPs. With our approach, NP dispersions of concentrations up to 30 mg/mL and good shelf-lifetime could be achieved, allowing the deposition of light-harvesting layers with less processing steps than reported before. Under thermal annealing, the ion pair formation process was reversible and AcOH was released. The performance of the corresponding bulk-heterojunction solar cells was similar to the performance of solar cells fabricated with the dispersions without the assistance of P3HT-PyH$^+$AcO$^-$ ion pair. We propose that this concept of end-capped polymeric additives, where the ionic form of the molecule switches to non-ionic form after thermal annealing, can be used as a universal approach to stabilize future bulk-heterojunction NP dispersions and hence substitute conventional surfactants without sacrificing solar cell performance.

4. Experiments

Materials

Unless noted otherwise, all materials were reagent grade and used as received without further purification. Anhydrous tetrahydrofuran, toluene, *o*-dichlorobenzene (DCB) were obtained by passing commercially available HPLC grade solvent through a Pure Processing Technology glass contour solvent purification system. P3HT (4002-EE, 50-70 kg/mol, RR 92%) was purchased from Rieke Metals. ICBA was purchased from Luminescence Technology Corp. Reagent grade chloroform and MeOH were used for NP formation.

Synthesis of P3HT-Py

Initially, P3HT with M_n = 5,000 g/mol was synthesized according to literature procedures.[24] Then we modified P3HT for pyridine end-capping. To a dry 100 mL Schlenk tube, 200 mg of P3HT (0.04 mmol, 1 eq.), 4.6 mg of $Pd(PPh_3)_4$ (0.004 mmol, 0.1 eq.), 164 mg of 4-pyridineboronic acid pinacol ester (0.8 mmol, 20 eq.) were added and degassed with nitrogen for 30 minutes. Meanwhile, dry THF and 2 M K_2CO_3 (aq.) were also degassed in respective round bottom flasks for 1 hour. After degassing, 10 mL of THF were added into the Schlenk tube followed by 4 mL of 2 M K_2CO_3 (aq.) (8 mmol) and the reaction mixture was heated overnight at 80 °C. The polymer P3HT-Py was subjected to preliminary purification steps - 1) liquid-liquid extraction of the polymer by washing thoroughly with water to remove unwanted salts, 2) filtering through silica to remove excess of Pd catalyst, and 3) Soxhlet extraction using acetone, petroleum ether and chloroform. To remove P3HT (H/H), the polymer was reacted with p-toluene sulfonic acid for 1 hour to generate P3HT-PyH^+TsO^-. After this, the resulting polymer was dry loaded to a silica column and eluted with chloroform. Fractions containing pyridinium salt were collected and the chloroform was completely evaporated. To regenerate P3HT-Py from P3HT-PyH^+TsO^-, the polymer was re-dissolved in small amount of THF and was reacted with NaOH (aq.). THF was removed from the resultant polymer and it was again dissolved in chloroform to wash thoroughly with water using liquid-liquid extraction technique. Only 26% of the pure P3HT-Py was obtained (53.2 mg, 0.01 mmol, 26%).

^{1}H NMR (400 MHz, $CDCl_3$): δ [ppm]= 8.7 (d, 2H), 7.4 (d, 2H), 7.0 (s, 28H), 2.6-2.8 (t, 60H), 1.7-1.4 (m, 302H), 1.4-0.9 (m, 112H).

GPC: M_n: 5,600 g/mol, M_w: 7,100 g/mol, M_z: 8,300 g/mol, $Đ$: 1.3

MS MALDI-TOF; m/z = 2240.7-3737.5 [Gaussian distribution differencing in mass of pyridine end-cap, M ± 78.03]

Synthesis of nanoparticles

To form NP dispersions using P3HT-Py, the amounts of both P3HT-Py and AcOH were varied with respect to the mass of P3HT. For example: to produce dispersions with a concentration of 1 mg/mL, 0.5 mg of each P3HT and ICBA were dissolved in chloroform. Targeting 3 wt.% of P3HT-Py and AcOH for NP stabilization, the amount of both P3HT-Py and AcOH required was 0.015 mg {(3×0.5)/100}. To add such small amounts, standard solutions of P3HT-Py and AcOH with concentrations of 3 mg/mL were prepared in $CHCl_3$ and MeOH, respectively. Then 5 µL of the P3HT-Py solution were added to the P3HT solution and 5 µL of the AcOH solution were added to the MeOH, in which the the NPs were formed.

P3HT (Rieke) and ICBA (1:1, wt:wt) as well as P3HT-Py were dissolved seperately in chloroform and then mixed (1 mg/mL) and heated to 56 °C on a hotplate. At the same time, AcOH (same mass as P3HT-Py, i.e., molecular excess of AcOH for best P3HT-Py ionization) was added into MeOH (non-solvent). Then MeOH was also heated to 56 °C, and the chloroform solution was injected into the MeOH (1:4, v:v) for an immediate reduction of the solubility of the semiconductor mixture and hence to form the NP dispersion under constant stirring (700 rpm). After NP formation, the beaker was removed from the hotplate and the stirrer bar was removed from the beaker to prevent aggregation of NPs. Finally, the volume of the NP dispersion was reduced by evaporating all of the solvent and some of the non-solvent in a water bath to produce a NP dispersion with the desired concentration. Higher concentrations of dispersions were facilitated by increasing the initial concentration of P3HT and ICBA in chloroform. For example: to synthesize 20 mg/mL dispersions, 10 mg each of P3HT and ICBA were dissolved in 1 mL of chloroform.

NP dispersions without assistance of P3HT-Py and AcOH were prepared following the similar procedure, except for the respective addition of P3HT-Py and AcOH into chloroform and methanol solution.

Device fabrication

OSCs with inverted device architecture were fabricated, see Figure 7A. Indium tin oxide (ITO) coated glass substrates were cleaned by ultrasonication in acetone and isopropanol (10 min each). The cleaned substrates were exposed to an oxygen plasma (10 min) to remove any organic traces. The zinc oxide (ZnO) electron transport layer was spin cast (3000 rpm, 30 s, 30 nm) from synthesized ZnO NP dispersions[25] onto the ITO electrode and annealed (150 °C, 10 min). P3HT:ICBA (1:1 wt:wt) dispersions of 10 mg/mL and 20 mg/mL in MeOH were spin cast 8 and 3 times for light-harvesting layer formation, respectively, and again annealed at 150 °C for another 10 min. Then the hole transport layer poly(3,4-ethylenedioxythiophene) : polystyrene sulphonate (PEDOT:PSS, Heraeus Clevios™ HTL Solar, 35 nm) was spin cast atop and annealed (150 °C, 5 min) in a glovebox,

followed by vacuum sublimation of a silver top electrode (Ag, 100 nm).

Another set of devices from 20 mg/mL dispersions were fabricated using the same conditions, but the NP films were solvent vapor annealed (THF, 20 s) followed by thermal annealing (150 °C, 10 min). The PEDOT:PSS was deposited on the light-harvesting layer and was annealed (150 °C, 10 min).

For reference, the P3HT:ICBA (1:1 wt:wt) light-harvesting layer was spin cast (1000 rpm, 30 s) from DCB solution onto the ZnO layer. Then the sample was annealed (150 °C, 5 min), followed by PEDOT:PSS and Ag deposition as described above.

Layer thicknesses were measured with a tactile stylus profiler (Dektak Profilometer Bruker).

ASSOCIATED CONTENT

Supporting Information

The Supporting Information is available free of charge on the ACS Publications website. Experimental details and plots of ^{1}H NMR, GPC, MALDI-TOF and DLS measurements. Tabular data of DLS results and UV-Vis plots of dispersions.

AUTHOR INFORMATION

Corresponding Author

* David J. Jones (djjones@unimelb.edu.au)
* Wallace W. H. Wong (wwhwong@unimelb.edu.au)

ACKNOWLEDGMENT

This work was made possible by support from the Australian Renewable Energy Agency (ARENA) which funds the project grants within the Australian Centre for Advanced Photovoltaics (ACAP). PM and AC thank the German Federal Ministry for Education and Research for support under contract 03EK3571 (project TAURUS 2). Extending thanks to Prof. Frank Caruso for allowing to use the Zetasizer for NP characterization. WWHW is supported by the ARC Centre of Excellence in Exciton Science (CE170100026).

ABBREVIATIONS

Organic Solar Cell, OSC; Nanoparticles, NP; Acetic acid, AcOH; Methanol, MeOH; *o-dichlorobenzene, DCB;* Poly-3-hexylthiophene, P3HT; Solvent vapor annealing, SVA; Thermal annealing, TA; Indene-C_{60} bis-adduct, ICBA; pyridine end-capped P3HT, P3HT-Py.

REFERENCES

1. Liu, Q.; Jiang, Y.; Jin, K.; Qin, J.; Xu, J.; Li, W.; Xiong, J.; Liu, J.; Xiao, Z.; Sun, K., 18% Efficiency Organic Solar Cells. *Sci. Bull.* **2020,** *65*, 272-275.
2. Cui, Y.; Yao, H.; Hong, L.; Zhang, T.; Tang, Y.; Lin, B.; Xian, K.; Gao, B.; An, C.; Bi, P., Organic Photovoltaic Cell with 17% Efficiency and Superior Processability. *Natl. Sci. Rev.* **2020,** *7*, 1239-1246.
3. Colsmann, A.; Röhm, H.; Sprau, C., Shining Light on Organic Solar Cells. *Solar RRL* **2020,** *4*, 2000015.
4. Sprau, C.; Buss, F.; Wagner, M.; Landerer, D.; Koppitz, M.; Schulz, A.; Bahro, D.; Schabel, W.; Scharfer, P.; Colsmann, A., Highly Efficient Polymer Solar Cells Cast from Non-Halogenated Xylene/Anisaldehyde Solution. *Energy Environ. Sci.* **2015,** *8*, 2744-2752.
5. Gartner, S.; Christmann, M.; Sankaran, S.; Rohm, H.; Prinz, E. M.; Penth, F.; Putz, A.; Tureli, A. E.; Penth, B.; Baumstummler, B.; Colsmann, A., Eco-Friendly Fabrication of 4% Efficient Organic Solar Cells from Surfactant-Free P3HT:ICBA Nanoparticle Dispersions. *Adv. Mater.* **2014,** *26*, 6653-6657.
6. Thalluri, G. K. V.; Bolsee, J.-C.; Gadisa, A.; Parchine, M.; Boonen, T.; D'Haen, J.; Boyukbayram, A. E.; Vandenbergh, J.; Cleij, T. J.; Lutsen, L., Opto-Electrical and Morphological Characterization of Water Soluble Conjugated Polymers for Eco-Friendly Hybrid Solar Cells. *Sol. Energy Mater. Sol. Cells* **2011,** *95*, 3262-3268.
7. Gärtner, S.; Reich, S.; Bruns, M.; Czolk, J.; Colsmann, A., Organic Solar Cells with Graded Absorber Layers Processed from Nanoparticle Dispersions. *Nanoscale* **2016,** *8*, 6721-6727.
8. Satapathi, S.; Gill, H. S.; Li, L.; Samuelson, L.; Kumar, J.; Mosurkal, R., Synthesis of Nanoparticles of P3HT and PCBM for Optimizing Morphology in Polymeric Solar Cells. *Appl. Surf. Sci.* **2014,** *323*, 13-18.
9. Vaughan, B.; Williams, E. L.; Holmes, N. P.; Sonar, P.; Dodabalapur, A.; Dastoor, P. C.; Belcher, W. J., Water-Based Nanoparticulate Solar Cells Using a Diketopyrrolopyrrole Donor Polymer. *Phys. Chem. Chem. Phys.* **2014,** *16*, 2647-2653.
10. Holmes, N. P.; Ulum, S.; Sista, P.; Burke, K. B.; Wilson, M. G.; Stefan, M. C.; Zhou, X.; Dastoor, P. C.; Belcher, W. J., The Effect of Polymer Molecular Weight on P3HT:PCBM Nanoparticulate Organic Photovoltaic Device Performance. *Sol. Energy Mater. Sol. Cells* **2014,** *128*, 369-377.
11. Ulum, S.; Holmes, N.; Barr, M.; Kilcoyne, A. L. D.; Gong, B. B.; Zhou, X.; Belcher, W.; Dastoor, P., The Role of Miscibility in Polymer:Fullerene Nanoparticulate Organic Photovoltaic Devices. *Nano Energy* **2013,** *2*, 897-905.
12. Xie, C.; Heumüller, T.; Gruber, W.; Tang, X.; Classen, A.; Schuldes, I.; Bidwell, M.; Späth, A.; Fink, R. H.; Unruh, T., Overcoming Efficiency and Stability Limits in Water-Processing Nanoparticular Organic Photovoltaics by Minimizing Microstructure Defects. *Nat. Commun.* **2018,** *9*, 1-11.
13. Dang, M. T.; Hirsch, L.; Wantz, G., P3HT:PCBM, Best Seller in Polymer Photovoltaic Research. *Adv. Mater.* **2011,** *23*, 3597-3602.
14. Zhao, G.; He, Y.; Li, Y., 6.5% Efficiency of Polymer Solar Cells Based on Poly (3-Hexylthiophene) and Indene-C_{60} Bisadduct by Device Optimization. *Adv. Mater.* **2010,** *22*, 4355-4358.
15. Darwis, D.; Holmes, N.; Elkington, D.; David Kilcoyne, A. L.; Bryant, G.; Zhou, X.; Dastoor, P.; Belcher, W., Surfactant-Free Nanoparticulate Organic Photovoltaics. *Sol. Energy Mater. Sol. Cells* **2014,** *121*, 99-107.
16. Sankaran, S.; Glaser, K.; Gärtner, S.; Rödlmeier, T.; Sudau, K.; Hernandez-Sosa, G.; Colsmann, A., Fabrication of Polymer Solar Cells from Organic Nanoparticle Dispersions by Doctor Blading or Ink-Jet Printing. *Org. Electron.* **2016,** *28*, 118-122.
17. Rashid, T.; Kait, C. F.; Murugesan, T., Effect of Alkyl Chain Length on the Thermophysical Properties of Pyridinium Carboxylates. *Chin. J. Chem. Eng.* **2017,** *25*, 1266-1272.
18. Loewe, R. S.; Ewbank, P. C.; Liu, J.; Zhai, L.; McCullough, R. D., Regioregular, Head-to-Tail Coupled Poly (3-Alkylthiophenes) Made Easy by the Grim Method: Investigation of the Reaction and the Origin of Regioselectivity. *Macromolecules* **2001,** *34*, 4324-4333.
19. Li, Y.; Vamvounis, G.; Yu, J.; Holdcroft, S., A Novel and Versatile Methodology for Functionalization of Conjugated Polymers. Transformation of Poly (3-Bromo-4-Hexylthiophene) Via Palladium-Catalyzed Coupling Chemistry. *Macromolecules* **2001,** *34*, 3130-3132.
20. Moulé, A. J.; Allard, S.; Kronenberg, N. M.; Tsami, A.; Scherf, U.; Meerholz, K., Effect of Polymer Nanoparticle Formation on the Efficiency of Polythiophene Based "Bulk-Heterojunction" Solar Cells. *J. Phys. Chem. C* **2008,** *112*, 12583-12589.
21. Nagarjuna, G.; Baghgar, M.; Labastide, J. A.; Algaier, D. D.; Barnes, M. D.; Venkataraman, D., Tuning Aggregation of Poly (3-Hexylthiophene) within Nanoparticles. *ACS nano* **2012,** *6*, 10750-10758.
22. Ulum, S.; Holmes, N.; Darwis, D.; Burke, K.; Kilcoyne, A. D.; Zhou, X.; Belcher, W.; Dastoor, P., Determining the Structural Motif of P3HT:PCBM Nanoparticulate Organic Photovoltaic Devices. *Sol. Energy Mater. Sol. Cells* **2013,** *110*, 43-48.
23. Gärtner, S.; Clulow, A. J.; Howard, I. A.; Gilbert, E. P.; Burn, P. L.; Gentle, I. R.; Colsmann, A., Relating Structure to

Efficiency in Surfactant-Free Polymer/Fullerene Nanoparticle-Based Organic Solar Cells. *ACS Appl. Mater. Interfaces* **2017,** *9*, 42986-42995.

24. Lin, Y.-H.; Smith, K. A.; Kempf, C. N.; Verduzco, R., Synthesis and Crystallinity of All-Conjugated Poly (3-Hexylthiophene) Block Copolymers. *Polym. Chem.* **2013,** *4*, 229-232.

25. Subbiah, J.; Purushothaman, B.; Chen, M.; Qin, T.; Gao, M.; Vak, D.; Scholes, F. H.; Chen, X.; Watkins, S. E.; Wilson, G. J.; Holmes, A. B.; Wong, W. W. H.; Jones, D. J., Organic Solar Cells Using a High-Molecular-Weight Benzodithiophene–Benzothiadiazole Copolymer with an Efficiency of 9.4%. *Adv. Mater.* **2015,** *27*, 702-705.

For Table of Contents Only